Article

by Siti Aisyah Nurjannah Et Al.

Submission date: 31-Jul-2023 10:21PM (UTC+0700)
Submission ID: 2139564917
File name: esm_2022_27.pdf (1.91M)
Word count: 7752
Character count: 38192

Engineering Solid Mechanics 11 (2023) 89-102

Contents lists available at GrowingScience

Engineering Solid Mechanics

homepage: www.GrowingScience.com/esm

The analysis of numerical self-compacting concrete wall panel models with variations of shear reinforcement

Siti Aisyah Nurjannah[a], Saloma[a*], Yulindasari[a], Kiagus Muhammad Aminuddin[a] and Gilbert Chuhairy[a]

[a]Civil Engineering Department, Faculty of Engineering, Universitas Sriwijaya, Indralaya 30662, Indonesia

ARTICLEINFO

Article history:
Received 18 January 2022
Accepted 26 June 2022
Available online
15 August 2022

Keywords:
Boundary element
Finite Element Method
Hysteretic curve
Reinforced concrete wall panel
Self-Compacting Concrete

ABSTRACT

Reinforced concrete wall critical zones are the responsive areas of dissipated earthquake loads. They are formed in the connection of the wall panels and the fixed restraints. The longitudinal and transversal steel reinforcements with certain spacing are designed according to the required nominal strength at the connections. Under certain conditions, the reinforcement distance becomes very tight, making working on castings using normal concrete difficult. This condition also occurs in boundary elements consisting of longitudinal and transversal reinforcements in tight spaces. A concrete material that flows easily and solidifies itself is required to avoid segregation. One type of this material is Self-Compacting Concrete (SCC). The SCC performance as a wall panel material that withstands gravity and cyclic lateral loads still require further research. This study aimed to analyze the hysteretic performance of reinforced SCC wall panels with variations of shear reinforcement in resisting cyclic lateral loads. The analysis used software based on numerical analysis. The drift ratios, hysteretic curves, stress patterns, ductility, and stiffness of the wall panels were analyzed. The SCC wall panel with ordinary shear reinforcement resisted lateral positive and negative loads of 152.32 kN and 143.09 kN, respectively. In comparison, the wall panel with boundary elements and tighter shear reinforcements could withstand the positive and negative lateral loads of 187.62 kN and 145.98 kN, respectively. The SCC wall panel reached the best ductility of 21.38 with ordinary shear reinforcement because the yield occurred faster than in other wall panels. The results showed that the boundary elements and shear reinforcements of reinforced SCC wall panels affected the performance in resisting cyclic lateral loads.

1. Introduction

The nonstructural masonry walls are usually made of bricks and have inadequate strength to resist earthquake loads. The behavior is brittle under compression and unable to resist tensile and shear forces. Earthquakes work as cyclic lateral loads that cause compressive and tensile forces on the walls. Structural wall panels that are made of reinforced concrete provide higher nominal strength than masonry walls in resisting earthquake loads. They have stiffness and strength that can withstand moments, axial, and shear forces. The connection between the wall panels and the fixed restraints resists the greatest moments due to the cyclic lateral loads. The spacing of longitudinal and shear reinforcements is adjusted according to the required nominal design capacity. The tight distances between steel reinforcement cause difficulties in pouring concrete mortar in the mold, resulting in segregation, and reducing strength. In the boundary elements consisting of longitudinal and transversal reinforcements in tight spaces, the concrete flow is also at risk of being obstructed. A material that flows easily fills the gaps between the reinforcement and solidifies itself is needed to avoid this lack. One of the materials that meet these properties is Self-Compacting Concrete (SCC) which can solidify due to its weight and gravity. It can fill the voids in formwork corners without vibration and compaction during the casting process (Li et al., 2021, Li et al., 2021). The SCC was developed in 1988 to produce better durability of concrete than normal concrete (Okamura & Ouchi, 2003, Nuruzzaman at al., 2022). The use of

* Corresponding author.
E-mail addresses: salomaunsri@gmail.com (Saloma)

ISSN 2291-8752 (Online) - ISSN 2291-8744 (Print)

doi: 10.5267/j.esm.2022.8.002

30% ground ferronickel slag and 50% ferronickel slag to replace binder cement and sand resulted in SCC as a high-strength concrete (Nuruzzaman et al., 2022). Ofuyatan et al. (2021) reported SCC as light-weight concrete with 1702 kg/m^3 to 1800 kg/m^3 of density and compressive strength that ranged from 23.88 MPa to 28.09 MPa. Some natural materials waste in industrial activities is part of SCC composition to support environmental sustainability. Commonly used materials in producing light-weight SCC are expanded clay, slag, perlite, and polymer (Vakhshouri and Nejadi, 2016). The use of light materials can decrease the gravity load and reduce the dimensions of the member structure, thereby lowering construction costs. Precast reinforced concrete (RC) wall panels are widely used to save construction work time, efficiently use materials and molds, be sustainable, maintain quality, and are environmentally friendly (Li et al., 2022; Khan et al., 2021). The function of RC wall panels in old constructions was only as a frame filler, but now it has become more important to become a load-bearing member (Abdel-Jaber and El-Nimri, 2022).

1.1 Research Significance

The behavior of wall panel members using SCC material and resisting cyclic lateral loads still needs further investigation. As the technology develops, research related to the examination of structural members is not only conducted experimentally in the laboratories. The studies are also available using software that is developed from a numerical approach of the finite element method. This study was intended to analyze the behavior of Self-Compacting Concrete wall panels with various shear reinforcements under cyclic lateral loads. The shear reinforcements included boundary elements. Boundary elements are one type of shear reinforcement that usually strengthens shear walls in critical areas on edge or outside reinforced concrete walls. The dimension of boundary elements and reinforcements space is usually very close, forming several layers of attached anchors that result in tighter spaces (AbdelRahman & Galal, 2021). The analysis results of the wall panels were hysteretic curves, story drifts, stress patterns, ductility, and stiffness degradation. The hysteresis curve is the most important characteristic for evaluating the seismic behavior of structural elements during the loading cycle. The hysteresis curves reflect the degradation of strength and stiffness, displacement, energy dissipation capacity, and ductility according to the lateral displacement in each cycle (Park, 1989, Ergun & Demir, 2015). Sengupta and Li (2014) used several hysteretic curve modeling methods and equations that experienced stiffness degradation and pinching. Hysteresis models could be classified into polygonal and smooth hysteretic models. In the polygonal hysteretic model, changes in stiffness were considered at the stages of crack, yield, strength, and stiffness degradation. In the smooth hysteresis models, the stiffness constantly changed due to yield and deterioration in unloading. The elastoplastic and degrading bilinear models did not match the structure specimen hysteresis curve. In comparison, the Bouc-Wen-Baber-Noori hysteretic model performed accurately with only a 3% deviation. Finite Element Analysis (FEA) is a simulation of dividing an object into smaller elements. It used a numerical method, the Finite Element Method (FEM), which can be a substitute for solving non-linear problems compared to experimental tests. In this study, the ANSYS software was used to solve the non-linear equations in the wall panel modeling.

1.2 Previous research on wall panels

Bai et al. (2021) conducted a study of performance comparison of wall panels of reinforced normal concrete and reinforced engineered cementitious composites panels with a dimension of 4350 mm × 4200 mm that were examined in an experimental program. The engineered cementitious composites significantly improved wall panel capacity, stiffness, and ductility. It indicated that materials other than normal concrete have the potential to be applied to form structural members. Zhang et al. (2021) proposed an infill wall panel equipped with damping for semi-rigid connected steel frames to reduce the interaction effect of infill wall panels that weaken the strength of the structure. The infill wall panel systems responded like plain trusses in terms of hysteretic behavior, reduced load bearing capacity, and displacement ductility. The system also increased about 23.3% of steel frame energy dissipation and relieved stress on columns. The analysis showed that the wall panels could be reinforced with a damping system to withstand cyclic lateral loads. Several studies about the influence of boundary elements on the masonry wall panels revealed the functions of postponing buckling of the longitudinal steel bars, increasing strength, stability, lateral capacity, enlarging curvatures, and ductility (Aly & Galal, 2020). Li et al. (2022) researched full-scale two precast hollow core wall panels, two precast reinforced concrete wall panels with boundary elements, and two non-hollow wall panels for comparison. It was reported that the hollow core reinforced concrete wall panel specimens with boundary elements performed better than the ordinary precast hollow core wall panels in resisting shears. The boundary elements provided the strength that led the wall panels to achieve one higher drift ratio than their non-hollow counterparts. The equipped boundary elements wall panels showed the relatively same lateral resistance and higher energy dissipation than the non-hollow ones. Gu et al. (2022) tested three T-shaped precast shear walls (TSWs) with boundary elements and columns and two reference TSWs to resist lateral cyclic loads. The experimental program revealed that the TSWs with boundary elements and columns with 0.2 $f_c' A_g$ compression load exhibited close performance to the reference counterparts. Even the boundary elements and columns with 0.4 $f_c' A_g$ compression load provided the strength that made the shear walls performed a similar or better performance than reference counterparts. These TSWs with boundary elements and columns also exhibited better seismic performance.

2. Materials and method

2.1 Concrete and Steel Bars

The material properties as input for modeling concrete and steel reinforcement are shown in Table 1. The Normal Concrete (NC) compressive strength (f_c') was 38.5 MPa and modulus of elasticity (E_c) was 12,600 MPa. The plain steel reinforcements

had a variation of diameter of 10 mm and 6 mm with the yield and ultimate strengths (f_y and f_u) (Lu & Henry, 2018). The Self-Compacting Concrete (SCC) properties were the compressive strength and modulus of elasticity of 41.813 MPa and 30,391 MPa, respectively (Hanafiah et al., 2017). Although the NC and SCC compressive strength difference was only 3.313 MPa, the modulus of elasticity values showed that SCC was stiffer than NC in the elastic condition.

Table 1. Concrete and steel bar properties

Type	f_c'	Longitudinal steel			Transversal steel		
		Type	f_y	f_u	Type	f_y	f_u
	(MPa)		(MPa)	(MPa)		(MPa)	(MPa)
C0	38.500	7 D10	300	409	19 R6-150	300.6	461.8
C1	41.813	7 D10	300	409	19 R6-150	300.6	461.8
C2	41.813	7 D10	300	409	19 R6-150 & 10 R6-90	300.6	461.8
C3	41.813	7 D10	300	409	19 R6-150 & 24 R6-60	300.6	461.8

2.2 The Details of Models and Boundary Conditions

The software elements in modeling wall panels were SOLID65, SOLID45, and LINK180, representing concrete, steel plates, and steel bars. Each element behaved in accordance with the reality-represented materials. There were four wall panel models using two types of concrete, various shear reinforcements including boundary elements, and shear spacing, as shown in Table 2 and Fig. 1 and Fig. 2 (redrawn).

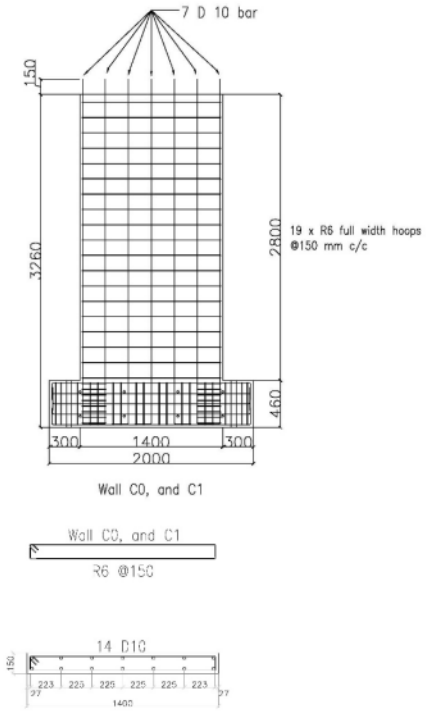

Fig. 1. The C0 and C1 wall panel models (Lu & Henry, 2018, redrawn)

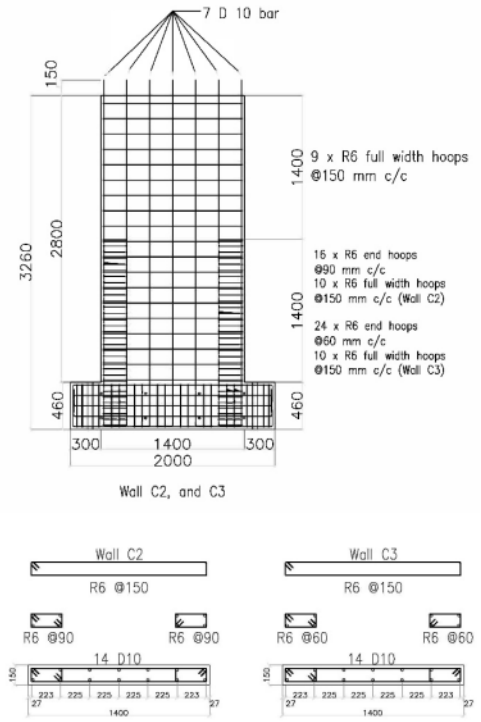

Fig. 2. The C2 and C3 wall panel models (Lu & Henry, 2018, redrawn)

The details of dimension and reinforcement were based on the experimental works of Lu & Henry (2018). Each wall panel model has a cross-sectional dimension of 150 mm x 1400 mm with a height of 3800 mm. The longitudinal reinforcement was D10 yield strength 300 MPa. The stirrup reinforcement of R6 @150 mm with a yield strength of 300.6 MPa. The width, height, and thickness of the wall panels were in the direction of the x, y, and z-axis as the software input. The boundary conditions are described as follows. The fixed restraints were in the bottom of wall panels that connected them with the foundations. The pinned restrained in the directions of three-axis were under the foundations. Then, the foundations did not move during the lateral cyclic loading. At the top of the wall, there were seven roll restraints in the z-direction (out of the wall plan), while the x and y axes were in free conditions. The cyclic lateral loading was carried out using a jack in the x-axis direction. The steel loading beam provided constant distributed loads in the y-axis direction. Four pins allowed the loading beam to move up and down in the y-axis direction.

Table 2. The shear reinforcement of the wall panel model

Wall panel model	Material	Shear reinforcements	Boundary element
C0	NC	19 × R6 @150	-
C1	SCC	19 × R6 @150	-
C2	SCC	9 × R6 @150	16 × R6 @90 and 10 × R6 @150
C3	SCC	9 × R6 @150	24 × R6 @60 and 10 × R6 @150

Note: NC: Normal Concrete, SCC: Self-Compacting Concrete

The nodes that formed elements of SOLID65, SOLID 45, and LINK180 (Gupta, 2020) are shown in Fig. 3. The nodes connected these elements to form the wall panel models and details. Fig. 4 shows the SOLID65 elements as NC and SCC materials as well as SOLID45, which formed the loading beam above the wall panel. Figs. 5, 6, and 7 show the LINK180 elements that formed the steel reinforcement of wall panel models C0 & C1, C2, and C3, respectively. The loading setup was based on the American Concrete Institute (2013) provision, as shown in Fig. 8.

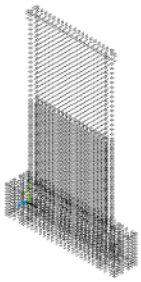

Fig. 3. The nodes that formed the elements

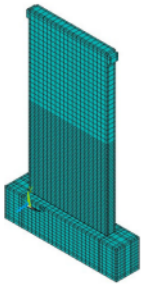

Fig. 4. The SOLID64 and SOLID45 elements of NC and SCC material modeling

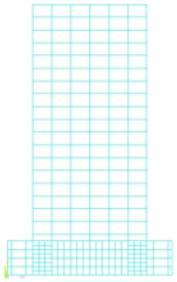

Fig. 5. The LINK180 elements of the C0 and C1 wall panel models

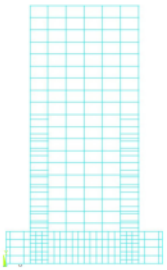

Fig. 6. LINK180 elements of the C2 wall panel model

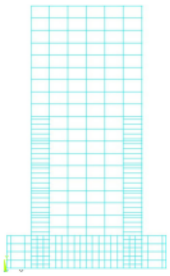

Fig. 7. LINK180 elements of the C3 wall panel model

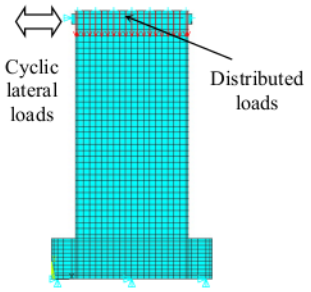

Fig. 8. Loading arrangement in the software

2.3 Lateral Cyclic Loading

The constant distributed load on the top of each wall panel was $0.15\ f_c^{'}A_g$ while the lateral cyclic load was a displacement control according to American Concrete Institute (2013) for experimental works. Budiono et al. (2019), Nurjannah et al. (2022), and Saloma et al. (2022) reported that three cycles of loads in each drift ratio of experimental works could be adapted into one cycle in the numerical analysis. The hysteretic curves of the first, second, and third cycle in the same drift ratio of the numerical analysis showed a similar shape and area. Then, it is allowed to simplify the three load cycles into one load cycle in all drift ratios. The loading cycle in the numerical analysis is shown in Fig. 9.

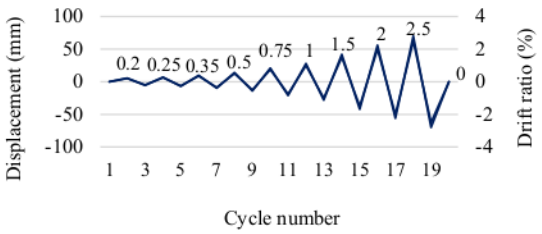

Fig. 9. The displacement history of lateral load cycles

3. Results and discussion

3.1. Comparison of the Experimental Program and Numerical Analysis

The numerical analysis results were hysteretic curves of lateral load and displacement relation. All lateral loads of numerical analysis were multiplied with a moment arm-length of 3.26 m based on the test set up in the experimental program (Lu & Henry, 2018). Then, it formed a hysteretic curve of moment and displacement relation. Each cyclic loading formed a loop of the hysteretic curve with peak moments or lateral loads due to positive and negative loads. The peak moments and correlated displacements of the C0 wall panel model were compared with the counterpart specimen for verification of numerical modeling. Tables 3 and 4 present the differences in the peak moments and correlated displacements between the C0 model and the specimen counterpart in the experimental program. Since the differences were less than 10%, the C0 wall panel model satisfied the accuracy (Wu et al., 2022). The moment and load types of hysteretic curves of the C0 model are shown in Fig. 10 and Fig. 11.

Table 3. The comparison of the peak moment of the C0 wall panel model and the specimen

Loading	Ratio drift	Moment		
		Numerical model	Specimen (Lu & Henry, 2018)	Difference
	(%)	(kN.m)	(kN.m)	(%)
Positive	1.5	491.83	485.70	1.26
Negative	1.5	-483.46	-490.20	1.38

Table 4. The comparison of displacement of the C0 wall panel model and the specimen

Loading	Ratio drift	Displacement		
		Model	Specimen (Lu & Henry, 2018)	Difference
	(%)	(mm)	(mm)	(%)
Positive	1.5	42.88	42.00	2.09
Negative	1.5	42.88	-42.00	2.10

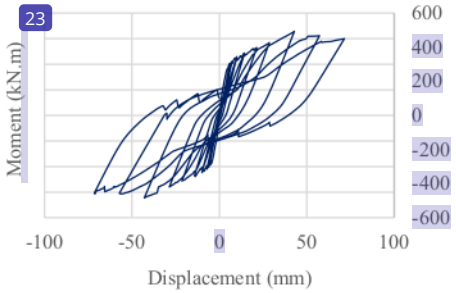

Fig. 10. The moment-displacement curve of the C0 model

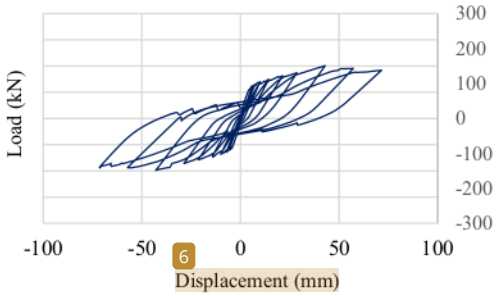

Fig. 11. The load-displacement curve of the C0 model

3.2 The Wall Panel Models Using Self-Compacting Concrete

Table 5 shows the peak lateral loads and displacement. The C1 model had the exact details of dimension and reinforcement as the C0 models.

Table 5. The peak lateral loads (F_p) and displacements (Δ_p) of SCC wall panel models

Loading	C1		C2		C3	
	F_p	Δ_p	F_p	Δ_p	F_p	Δ_p
	(kN)	(mm)	(kN)	(mm)	(kN)	(mm)
Positive	152.32	42.92	177.97	43.00	187.62	57.246
Negative	-143.09	-42.92	-145.67	-56.62	-145.98	-42.377

The difference was that the C0 model used Normal Concrete (NC), while the C1 model used Self-Compacting Concrete (SCC). The shear reinforcements of the SCC wall panel models were varied into three types. The performance of the wall panels, including the achieved lateral loads related to the strength, was influenced by the detail of each shear reinforcement. The maximum lateral load of the C1 model was less than the C2 and C3 models under positive and negative load directions. The C1 wall panel shear reinforcement of 19 × R6 @150 along 2800 mm of height achieved the maximum positive and negative loads of 152.32 kN and 143.09 kN, respectively. The tighter spacing of steel reinforcement of the C2 model in 1400

mm height of 9 × R6 @150 and 1400 mm height of 16 R6 @90 boundary element provided higher nominal strength than the C1 model. The C2 model achieved maximum lateral loads of 177.97 and 145.67 under positive and negative loads. The C3 model performed the best strength with maximum lateral loads of 187.62 and 145.977 under positive and negative load directions. This condition was due to the stronger provided nominal shear strength of the 1400 mm height of 9 × R6 @150 and 1400 mm height of 16 R6 @60 boundary element.

The different maximum displacement values of the C1, C2, and C3 models were correlated with the drift ratios in Table 6.

Table 6. The drift ratios on the peak lateral loads

Loading	Type		
	C1	C2	C3
	Drift ratio (%)	Drift ratio (%)	Drift ratio (%)
Positive	1.5	2.0	2.0
Negative	-1.5	-1.5	-1.5

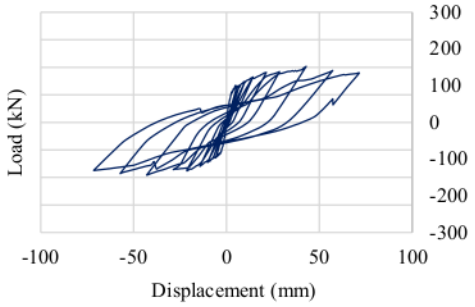

Fig. 12. The C1 wall panel model curve

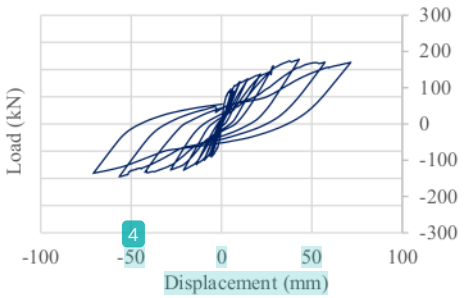

Fig. 13. The C2 wall panel model curve

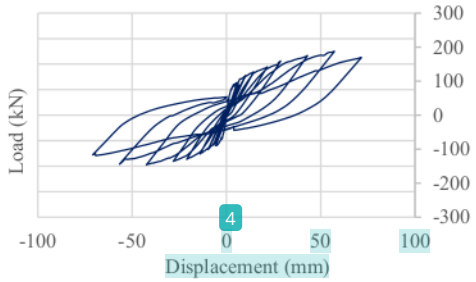

Fig. 14. The C3 wall panel model curve

The higher provided nominal shear strength of C2 and C3 than C1 models made them reach story drifts of 2.0% and 1.5%, while the C1 model only reached story drifts of 1.5% both under positive and negative loads, respectively. The C2 and C3 models experienced cracks on the concrete and yield on the steel bars under positive loads in story drifts of 2.0%, affecting the stiffness and strength. This condition made the C2 and C3 models only achieve the maximum story drift of 1.5% under negative loads. Fig. 12 presents the hysteretic curve of the C1 wall panel model. The shape of the curve shows adequate energy dissipation without pinching from the initial until ultimate loading. The C2 and C3 wall panel models in Fig. 13 and Fig. 14 also show the same energy dissipation behavior. There was no pinching in all models that indicated fully bonded steel bars on the concrete.

Table 7. Peak lateral loads

Loading	C0	C1	Difference
	Maximum lateral load (kN)	Maximum lateral load (kN)	(%)
Positive	150.87	152.32	0.95
Negative	-148.30	-143.09	3.64

The difference between achieved maximum story drift and maximum lateral loads resulted in the highest energy dissipation of the C3 model, followed by the C2 and C1 models, respectively. The C1 wall panel model using SCC material showed

relatively the same strength as the C0 model of NC material. The difference between peak lateral loads due to positive and negative loads was 0.95% and 3.64%, respectively, which is shown in Table 7. This behavior indicated that the SCC materials provided relatively close compression and tensile strength with NC. Thus, the SCC could potentially be applied as the material for a structural member of wall panels.

3.3 Stress Patterns

The distributed gravity and lateral cyclic loads resulted in compression and tension on the wall panels. The stress pattern was influenced by the nominal shear strength and the reinforcement details of each wall panel. Fig. 15 to Fig. 22 show wall panel stress patterns in the ultimate drift ratio of 2.50%. Fig. 15 shows the C0 wall panel under positive load had dominant compressive stress ranging from -6.333 MPa to -1.556 MPa (yellow) in the left half height from the bottom and top right regions.

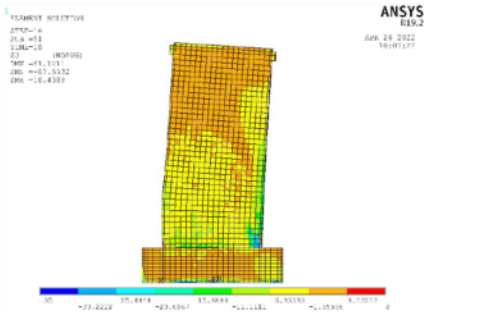

Fig. 15. Stress pattern of C0 wall panel; positive load

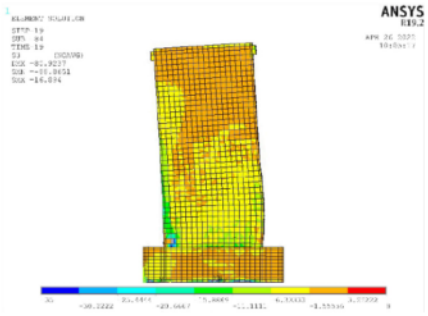

Fig. 16. Stress pattern of C0 wall panel; negative load

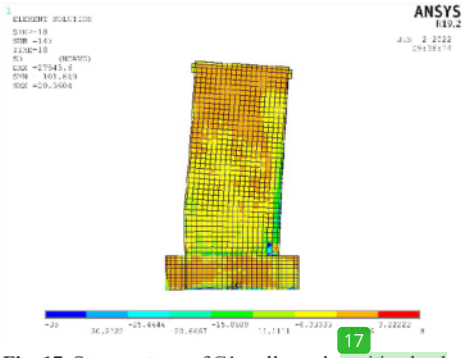

Fig. 17. Stress pattern of C1 wall panel; positive load

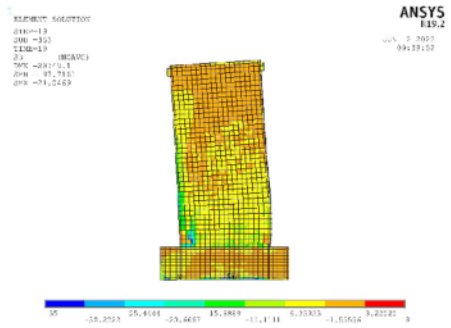

Fig. 18. Stress pattern of C1 wall panel; negative load

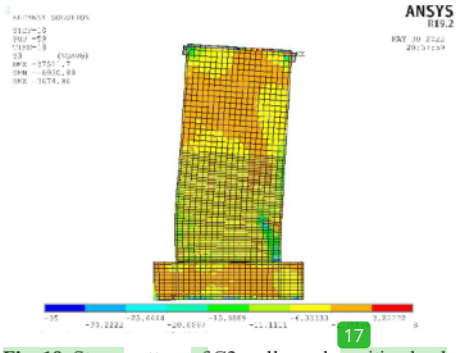

Fig. 19. Stress pattern of C2 wall panel; positive load

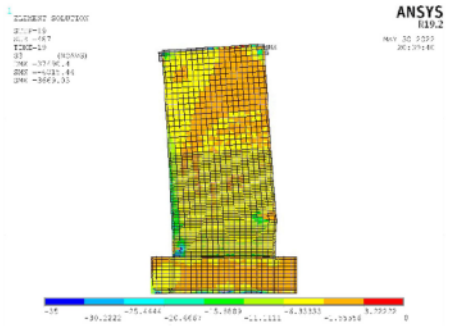

Fig. 20. Stress pattern of C2 wall panel; negative load

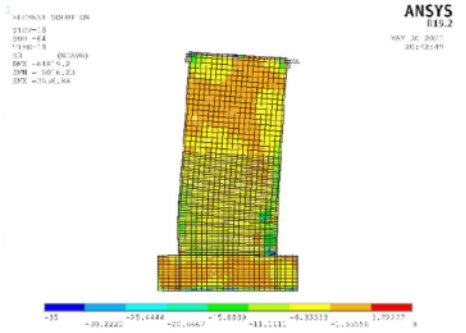

Fig. 21. Stress pattern of C3 wall panel; positive load

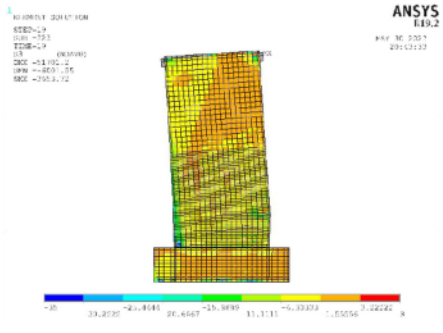

Fig. 22. Stress pattern of C3 wall panel; negative load

The left half top sections were dominated by compression stress of -1.556 MPa to a tensile stress of 3.222 MPa (orange). The outermost right side experienced higher compression stress that ranged from -15.889 MPa to -6.333 MPa (green and light green) due to the positive loads. The highest compression stress occurred on the right-side connection of the wall and foundation, ranging from -20.667 MPa (light blue) to 35 MPa (dark blue). The C0 wall panel's opposite behavior under negative loads in Figure 16. The dominant compressive stress of -6.333 MPa to -1.556 MPa spread from the bottom right-side to the right half height from the bottom to the left top region. The compression stress of -15.889 MPa to -6.333 MPa (green and light green) occurred along the outermost left half height from the bottom side of the wall panel. The highest compressive stress occurred in the connection of the wall and foundation on the left bottom side and ranged from -20.667 MPa to -35 MPa (light blue and dark blue).

Similar behavior was shown by the C1, C2, and C3 wall panel models under positive and negative loads in Fig. 17 to Fig. 22. The wall panel model types C1, C2, and C3 could withstand a tensile stress of 3.222 MPa and compressive stress of up to -30.22 MPa. However, there are differences in the stress pattern of each model. In the connection of the wall and foundation, the dark blue area, which showed the compressive stress of -30.22 MPa to -35 MPa of the C3 wall panel, was larger than the other types (Fig. 21 and Fig. 22). It was due to the additional boundary element shear reinforcement of 24 × R6 @60 mm boundary element that provided the highest shear nominal strength than other models. The dark blue areas of compression stress were followed by the wall panel model of C2 that was reinforced by the 16 × R6 @90 mm boundary element (Fig. 19 and Fig. 20). The C0 and C1 wall panels had the same compression areas of -30.22 MPa to -35 MPa and were wider than the C2 wall panel (Fig. 15 toFig. 18). This behavior was because these two wall panels were only reinforced by ordinary shear reinforcements of 19 × R6 @150. These different dark blue areas were influenced by the details of shear reinforcements and occurred under positive and negative loads. As the most compressed region, the bottom side of the wall panel always resisted dominant compressive stress under positive and negative loads. The outermost left sides experienced lower compression than the right side regions under positive loads (Fig. 15, Fig. 17, Fig. 19, and Fig. 21), while the opposite occurred under negative loads (Fig. 16, Fig. 18, Fig. 20, and Fig. 22).

3.4 Displacement Ductility

Ductility is the ability of material or structure in an inelastic condition to resist loads. There are several types of ductility: strain, rotation, displacement, and curvature (Park & Paulay, 1991). According to FEMA 356 (2000), the low, medium, and high ductility have values less than or equal to 2; between 2 and 4; and more or equal to 4, respectively. This study was focused on the influence of lateral drifts on the wall panel behavior, the type of analyzed ductility was the displacement one. The displacement ductility is the ratio between maximum displacements to the yield conditions. The yield points were determined using the provision of FEMA 356 (2000). Each drift ratio peak point formed skeleton curves representing the strength of wall panels. The regions formed by the skeleton curve and the two lines with certain slopes must have the same area. The skeleton curve was formed from the points when the maximum displacements occurred in each drift ratio due to positive and negative loads. The intersection of the two lines was the yield point. The determination of the location of the yield points of the C0 wall panel model using Normal Concrete (NC) is shown in Figure 23. Figures 24 to 26 show the skeleton curves and determination of the yield points of the C1, C2, and C3 wall panel models using Self-Compacting Concrete material (SCC). All displacements of yield, peak, and maximum condition are presented in Δ_y, Δ_p, and Δ_m, respectively. Loads of yield, peak, and maximum condition are expressed in F_y, F_p, and F_m, respectively. Both C0 and C1 models achieved maximum drift ratios of 1.5% under positive and negative loads. It was due to the same reinforcement details and relatively same concrete strengths of these models. The C2 and C3 were reinforced with boundary elements that confined concrete. Then they achieved the peak loads in drift ratios of 2.0% and 1.5% under positive and negative loads, respectively.

Table 8 shows the ductility of all models. Under positive loads, the C0 and C1 wall panels' yield displacements were relatively the same, i.e., 4.41 and 4.47, respectively. It indicated that the NC and SCC materials provided nearly performance of compression strength and were following properties in Table 1. The C2 and C3 models achieved higher yield displacements

than C0 and C1, i.e., 4.53 mm and 4.58 mm, respectively. The same behavior occurred under the negative loads. The C0 and C1 wall panel models yielded near values of 2.64 mm and 2.67 mm, while the C2 and C3 models yielded slower with displacements of 3.21 mm and 3.56 mm. All yield displacements under negative loads were less than positive loads due to cracks that decreased the strength of the wall panels.

The maximum displacements of all models were obtained from the numerical software output and based on the loading protocol in Fig. 9. It was a displacement control loading, then resulted in relatively the same maximum displacement on all wall panels in Table 8. Due to the positive and negative loads, the ductility of C0 was less than the C1 wall panel. It showed that NC was stiffer than SCC in resisting lateral positive and negative loads. The C2 wall panel that was reinforced by boundary elements and closer spacing of shear reinforcement than C0 and C1 performed less ductility due to the increased stiffness from the steel bars confinement. Then, the C3 models that had boundary elements and closer spacing of shear reinforcement than C2 achieved less ductility. The average values ranged from 17.76 to 21.62. This indicates that all models achieved high ductility.

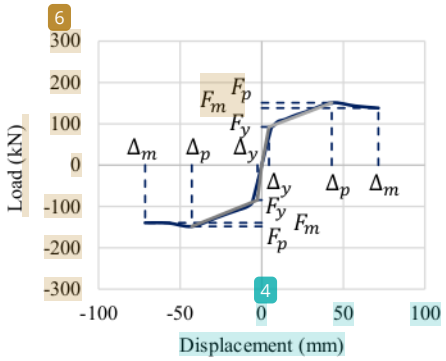

Fig. 23. The skeleton curve of the C0 wall panel

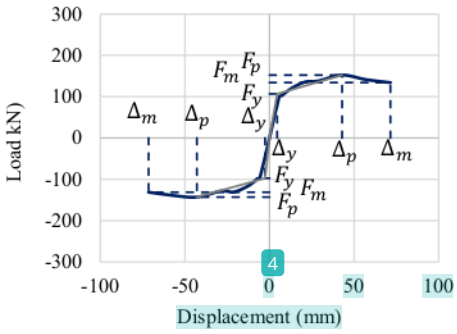

Fig. 24. The skeleton curve of the C1 wall panel

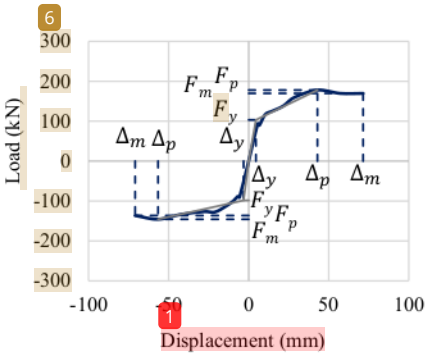

Fig. 25. The skeleton curve of the C2 wall panel

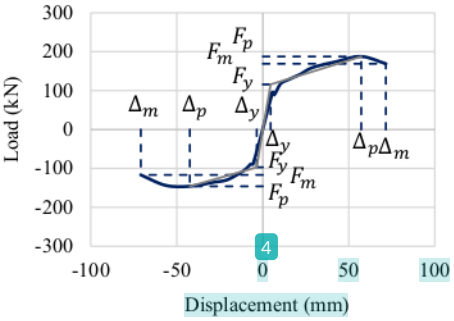

Fig. 26. The skeleton curve of the C3 wall panel

Table 8. Displacement ductility of the NC and SCC wall panel models

Type	Material	Load direction	Maximum displacement	Yield displacement	Ductility	Average ductility
			Δ_m (mm)	Δ_y (mm)	$\mu = \Delta_m/\Delta_y$	$\bar{\mu}$
C0	NC	+	71.47	4.41	16.20	21.62
		-	71.47	2.64	27.04	
C1	SCC	+	71.47	4.47	15.98	21.38
		-	71.48	2.67	26.78	
C2	SCC	+	71.52	4.53	15.79	18.93
		-	70.87	3.21	22.08	
C3	SCC	+	71.51	4.58	15.60	17.76
		-	70.89	3.56	19.91	

Note: +: positive; -: negative

3.5 Stiffness degradation

The stiffness is the lateral load and displacement ratio as secant stiffness (Zhang et al., 2021). The curve that presents the correlation of stiffness and drift ratio shows the behavior of wall panels in resisting lateral loads. The stiffness curves of C0, C1, C2, and C3 wall panels under positive and negative loads are shown in Figures 27 and 28. In the initial drift ratio of 0.2%, the C3 wall panel with the greatest area of shear reinforcements performed the highest stiffness of 16.722 kN/mm under positive load. The C2, C1, and C0 wall panels followed with 16.506, 16.282, and 15.810 kN/mm stiffness. It indicated that boundary elements and shear reinforcements influenced the stiffness in the initial positive loading.

The stiffness decreased almost simultaneously and significantly as the drift ratio increased. At a drift ratio of 0.75%, the difference in stiffness was obvious where C2, C1, and C0 wall panels achieved stiffnesses of 6.531, 6.372, 5.906, and 5.707 kN/mm, respectively. The behavior of the wall panel changed at a drift ratio of 1.00%, where C3 had the highest stiffness and was followed by C3, C0, and C1 wall panels at 5.558, 5.512, 4.546, and 4.481 kN/mm. At the end of the loading, when the drift ratio was 2.50%, the stiffnesses of C2, C3, C0, and C1 wall panels were 2.370, 2.358, 1.901, and 1.744 kN/mm. Since the drift ratio of 1.00% to 2.50%, the C2 and C3 wall panels performed almost the same stiffness behavior because of the type of same boundary elements and shear reinforcements with different spacing. The C0 and C1 wall panels also showed the same behavior that was influenced by the same shear reinforcements with different concrete materials.

With the initial drift ratio 0.20% under tensile load, the C3, C2, C1, and C0 wall panels had the same relative stiffness of 15.954, 15.896, 15.689, and 15.673 kN/mm. The stiffness decreased as the drift ratio increased. The difference in stiffness started to become obvious in the drift ratio of 0.50%. The C3 wall panel with the tightest confinement of boundary elements and shear reinforcements reached the highest stiffness of 8.173 kN/mm. The C2, C1, and C0 wall panels followed with 8.043 kN/mm, 7.802 kN/mm, and 7.573 kN/mm stiffness, respectively. All wall panels experienced decreased stiffness until the end of tensile loading in a drift ratio of 2.50%.

Under tensile load in the 0.20% initial drift ratio, the C3, C2, C1, and C0 wall panels had the same relative stiffnesses of 15.954, 15.896, 15.689, and 15.673 kN/mm. Then, the stiffness decreased as the drift ratio increased. The difference in stiffness was obvious in the story drift of 0.50%. The C3 wall panel with the tightest confinement of boundary elements and shear reinforcement achieved the highest stiffness of 8.173 kN/mm. The C2, C1, and C0 wall panels followed with 8.043 kN/mm, 7.802 kN/mm, and 7.573 kN/mm stiffness, respectively. All wall panels experienced decreased stiffness until the end of tensile loading with a drift ratio of 2.50%.

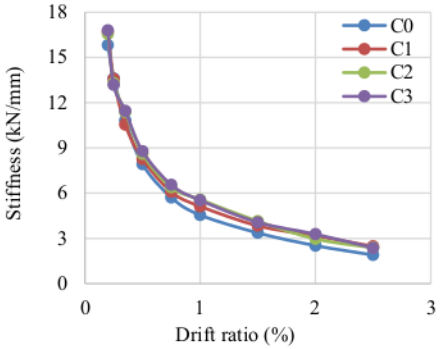

Fig. 27. Stiffness degradation curve of wall panels under the positive loads

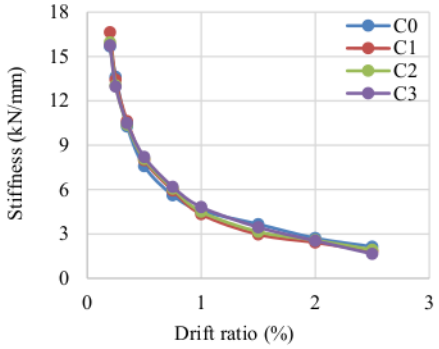

Fig. 28. Stiffness degradation curve of wall panels under the negative loads

Table 9 shows the stiffness degradation due to the positive loads on all models. The stiffness degradation of the C3 wall panel was the highest compared with the others in the initial drift ratio of 0.20%. It was 21.581 %, followed by the C2, C0, and C1 wall panels of 19.706, 13.960, and 12.034 %. The lower stiffness of the C1 wall panel than the C0 counterpart showed that in the 0.20% drift ratio under positive load, the NC material provided more stiffness than SCC. The stiffness degradation continued until the maximum drift ratio of 2.50 %, where the C1 wall panel was 89.291 %, followed by C0, C3, and C2 wall panels' of 87.975, 85.898, and 85.639 %.

Under the negative loads, the wall panels showed different behavior, as is shown in Table 10. The highest stiffness degradation occurred on the C1 wall panel at 18.403% in a drift ratio of 0.25%. The C2, C3, and C0 followed C1 with stiffness degradations of 18.249 %, 17.767 %, and 13.110%. The NC material performed higher stiffness than SCC in this drift ratio. It was shown by the stiffness degradation of C0 and C1 wall panels. All wall panels experienced stiffness

degradation until the maximum drift ratio of 2.50%, with values of 89.714 %, 89.126 %, 87.924 %, and 86.371 % for C3, C1, C2, and C0 wall panels, respectively.

Table 9. The stiffness degradation due to the positive loads

	C0		C1		C2		C3	
Drift ratio (%)	Stiffness (kN/mm)	Degradation (%)	Stiffness (kN/mm)	Degradation (%)	Stiffness (kN/mm)	Degradation (%)	Stiffness (kN/mm)	Degradation (%)
0.20	15.810	0	16.282	0	16.506	0	16.722	0
0.25	13.603	-13.960	14.322	-12.034	13.253	-19.706	13.113	-21.581
0.35	10.830	-31.497	10.393	-36.168	11.342	-31.281	11.421	-31.702
0.50	7.915	-49.934	8.041	-50.616	8.584	-47.995	8.75	-47.675
0.75	5.707	-63.902	5.906	-63.724	6.372	-61.394	6.531	-60.944
1.00	4.546	-71.243	4.481	-72.477	5.558	-66.327	5.512	-67.037
1.50	3.364	-78.724	3.301	-79.727	4.132	-74.968	4.055	-75.753
2.00	2.515	-84.091	2.294	-85.913	2.961	-82.063	3.270	-80.443
2.50	1.901	-87.975	1.744	-89.291	2.370	-85.639	2.358	-85.898

Table 10. The stiffness degradation due to the negative loads

	C0		C1		C2		C3	
Drift ratio (%)	Stiffness (kN/mm)	Degradation (%)	Stiffness (kN/mm)	Degradation (%)	Stiffness (kN/mm)	Degradation (%)	Stiffness (kN/mm)	Degradation (%)
0.20	15.673	0	15.689	0	15.896	0	15.954	0
0.25	13.618	-13.110	12.801	-18.403	12.995	-18.249	12.899	-17.767
0.35	10.261	-34.532	10.138	-35.381	10.352	-34.879	10.443	-33.421
0.50	7.573	-51.684	7.802	-50.268	8.043	-49.400	8.173	-47.897
0.75	5.607	-64.226	5.681	-63.791	6.046	-61.965	6.162	-60.717
1.00	4.568	-70.853	4.171	-73.412	4.487	-71.775	4.802	-69.388
1.50	3.659	-76.655	3.101	-80.237	3.139	-80.253	3.436	-78.092
2.00	2.714	-82.685	2.261	-85.590	2.568	-83.848	2.529	-83.878
2.50	2.136	-86.371	1.706	-89.126	1.920	-87.924	1.641	-89.714

4. Conclusion

The modeling of the C0, C1, C2 and C3 wall panels with materials of NC and SCC and variations of shear reinforcement and boundary elements in resisting cyclic lateral and uniform gravity loads has been analyzed to result in several conclusions as follows:

1. The difference in lateral loads and displacements between the C0 wall panel model and the specimen counterpart were 1.263%, 1.375%, 2.086%, and 2.096% due to positive and negative loads, respectively. Since all differences did not exceed 10%, the modeling method fulfills the accuracy requirement and is sufficient to be applied to the C1, C2, and C3 wall panels.
2. When the peak positive and negative loads occurred, the NC-C0 and SCC-C1 wall panels had a drift ratio of 1.5%. This condition showed that the SCC material had relatively the same performance as NC in resisting cyclic loads. The C2 and C3 wall panels achieved the peak positive loads at a drift ratio of 2.0% because of tighter boundary elements and shear reinforcements than the C0 and C1 wall panels. The damage in the form of concrete cracks resulted in C2 and C3 wall panels only reaching a 1.5% drift ratio at peak negative loads.
3. The SCC-C3 wall panel model performed a higher lateral load-resisting strength than the SCC-C1 and SCC-C2 wall panels. Details of shear reinforcement supported this condition. The C1 wall panel was only strengthened by shear reinforcements of 19 R6 @150 mm, while the C2 and C3 wall panels were confined by 19 R6 @150 mm and boundary elements with different spacing of 16 R6 @ 90 mm and 24 R6 @ 60 mm, respectively. The closer spacing of the C3 wall panel provided stronger confinement and increased resistance to lateral loads.
4. The NC-C0 wall panel's ductility of 21.62 was the highest compared with the SCC-C1 counterpart. This behavior shows that NC materials are more ductile than SCC. However, the SCC-C1, SCC-C2, and SCC-C3 wall panels achieved high ductility of 21.382, 18.933, and 17.758, respectively. The confinement of boundary elements and closer spacing made the SCC-C3 wall panel stiffer and experienced a slower yield than the others.

Acknowledgment

The authors gratefully acknowledge Sriwijaya University for its support of this research.

References

Abdel-Jaber, M., & El-Nimri, R. (2022). Comparative investigation, numerical modeling, and buckling analysis of one-way reinforced concrete wall panels. *Results in Engineering*, 100459. https://doi.org/10.1016/j.rineng.2022.100459

AbdelRahman, B., & Galal, K. (2021). Experimental investigation of axial compressive behavior of square and rectangular confined concrete-masonry structural wall boundary elements. *Engineering Structures*, *243*, 112584. https://doi.org/10.1016/j.engstruct.2021.112584

Aly, N., & Galal, K. (2020). Experimental investigation of axial load and detailing effects on the inelastic response of reinforced-concrete masonry structural walls with boundary elements. *Journal of Structural Engineering*, *146*(12), 04020259. https://doi.org/10.1061/(ASCE)ST.1943-541X.0002842

American Concrete Institute (ACI). (2013). Guide for Testing Reinforced Concrete Structural Elements Under Slowly Applied Simulated Seismic Loads, ACI 374.2 R13.

Bai, L., Hou, C., Cao, M., Hu, J., Zhou, T., & Wei, H. (2021). Cyclic performance of steel moment frames with prefabricated RC and ECC wall panels. *Engineering Structures*, *242*, 112492. https://doi.org/10.1016/j.engstruct.2021.112492

Budiono, B., Nurjannah, S. A., & Imran, I. (2019). *Non-linear Numerical Modeling of Partially Pre-stressed Beam-column Sub-assemblages Made of Reactive Powder Concrete*. Bandung Institute of Technology. https://doi.org/10.5614/j.eng.technol.sci.2019.51.1.3

Ergun, S., & Demir, A. (2015). Effect of hysteretic models on seismic behavior of existing RC structures. *Journal of Performance of Constructed Facilities*, *29*(6), 04014160. https://doi.org/10.1061/(ASCE)CF.1943-5509.0000653

FEMA 356, F. E. (2000). Prestandard and commentary for the seismic rehabilitation of buildings. *Federal Emergency Management Agency: Washington, DC, USA*.

Gu, Q., Zhao, D., Li, J., Peng, B., Deng, Q., & Tian, S. (2022). Seismic performance of T-shaped precast concrete superposed shear walls with cast-in-place boundary columns and special boundary elements. *Journal of Building Engineering*, *45*, 103503. https://doi.org/10.1016/j.jobe.2021.103503

Gupta, L. M., Ray, M. R., & Labhasetwar, P. K. (Eds.). (2020). *Advances in Civil Engineering and Infrastructural Development: Select Proceedings of ICRACEID 2019*. Springer.

Hanafiah, Saloma, & Whardani, P. N. K. (2017, November). The behavior of self-compacting concrete (SCC) with bagasse ash. In *AIP Conference Proceedings* (Vol. 1903, No. 1, p. 050005). AIP Publishing LLC. https://doi.org/10.1063/1.5011544

Khan, S. A., Koç, M., & Al-Ghamdi, S. G. (2021). Sustainability assessment, potentials and challenges of 3D printed concrete structures: A systematic review for built environmental applications. *Journal of Cleaner Production*, *303*, 127027. https://doi.org/10.1016/j.jclepro.2021.127027

Li, J., Tan, D., Zhang, X., Wan, C., & Xue, G. (2021). Mixture design method of self-compacting lightweight aggregate concrete based on rheological property and strength of mortar. *Journal of Building Engineering*, *43*, 102660. https://doi.org/10.1016/j.jobe.2021.102660

Li, J., Zhao, E., Niu, J., & Wan, C. (2021). Study on mixture design method and mechanical properties of steel fiber reinforced self-compacting lightweight aggregate concrete. *Construction and Building Materials*, *267*, 121019. https://doi.org/10.1016/j.conbuildmat.2020.121019

Li, W., Lin, X., Bao, D. W., & Xie, Y. M. (2022, April). A review of formwork systems for modern concrete construction. In *Structures* (Vol. 38, pp. 52-63). Elsevier. https://doi.org/10.1016/j.istruc.2022.01.089

Li, Y., Li, Z., Tang, Z., Xu, L., Wang, W., Yang, X., & Chen, Y. (2022). Seismic behaviour of a novel hollow-core precast shear wall with cast-in-situ boundary elements. *Journal of Building Engineering*, *52*, 104469. https://doi.org/10.1016/j.jobe.2022.104469

Lu, Y., & Henry, R. S. (2018). Comparison of minimum vertical reinforcement requirements for reinforced concrete walls. *ACI Structural Journal*, *115*(3), 673-687. https://doi.org/10.14359/51701146

Nurjannah, S., Saloma, S., Idris, Y., Usman, A., Juliantina, I., & Aprilia, C. (2022). The Behavior of Interior Beam-Column Joint Models Using Self-Compacting Concrete with Variations of Shear Reinforcement Subjected to Cyclic Lateral Loads. *Civil Engineering and Architecture 10*(4): 1574-1589. https://doi.org/10.13189/cea.2022.100427

Nuruzzaman, M., Kuri, J. C., & Sarker, P. K. (2022). Strength, permeability and microstructure of self-compacting concrete with the dual use of ferronickel slag as fine aggregate and supplementary binder. *Construction and Building Materials*, *318*, 125927. https://doi.org/10.1016/j.conbuildmat.2021.125927

Ofuyatan, O. M., Olutoge, F., Omole, D., & Babafemi, A. (2021). Influence of palm ash on properties of light weight self-compacting concrete. *Cleaner Engineering and Technology*, *4*, 100233. https://doi.org/10.1016/j.clet.2021.100233

Okamura, H., & Ouchi, M. (2003). Self-compacting concrete. *Journal of advanced concrete technology*, *1*(1), 5-15. https://doi.org/10.3151/jact.1.5

Park, R., & Paulay, T. (1991). *Reinforced concrete structures*. John Wiley & Sons.

Park, R. (1989). Evaluation of ductility of structures and structural assemblages from laboratory testing. *Bulletin of the new Zealand society for earthquake engineering*, *22*(3), 155-166. https://doi.org/10.5459/bnzsee.22.3.155-166

Saloma, S., Nurjannah, S., Usman, A., Idris, Y., Juliantina, I., & Effendy, R. (2022). The behavior of self compacting concrete exterior beam-column joints with a variation of shear reinforcement against cyclic lateral loads. *Engineering Solid Mechanics*, *10*(4), 373-386. https://doi.org/10.5267/j.esm.2022.6.001

Sengupta, P., & Li, B. (2017). Hysteresis modeling of reinforced concrete structures: state of the art. *ACI Structural Journal*, *114*(1), 25-38. https://doi.org/10.14359/51689422

Vakhshouri, B., & Nejadi, S. (2016). Mix design of light-weight self-compacting concrete. *Case Studies in Construction Materials*, *4*, 1-14. http://dx.doi.org/10.1016/j.cscm.2015.10.002

Wu, H., Zhuang, X., Zhang, W., & Zhao, Z. (2022). Anisotropic ductile fracture: Experiments, modeling, and numerical simulations. *Journal of Materials Research and Technology*. https://doi.org/10.1016/j.jmrt.2022.07.128

Zhang, C., Huang, W., Wang, H., & Gao, J. (2021). Experimental and numerical study on seismic performance of semi-rigid steel frame infilled with prefabricated damping wall panels. *Engineering Structures*, *246*, 113056. https://doi.org/10.1016/j.engstruct.2021.113056

Article

ORIGINALITY REPORT

9%	6%	5%	1%
SIMILARITY INDEX	INTERNET SOURCES	PUBLICATIONS	STUDENT PAPERS

PRIMARY SOURCES

1	www.m.growingscience.com Internet Source	1%
2	www.growingscience.com Internet Source	1%
3	www.hrpub.org Internet Source	1%
4	wcee.nicee.org Internet Source	1%
5	Li Yanna, Li Zhenbao, Tang Zhenyun, Xu Liangyu, Wang Wei, Yang Xiaohong, Chen Youfan. "Seismic behaviour of a novel hollow-core precast shear wall with cast-in-situ boundary elements", Journal of Building Engineering, 2022 Publication	<1%
6	www.j-act.org Internet Source	<1%
7	unsworks.unsw.edu.au Internet Source	<1%

8	Nurjannah Aisyah, S Saloma, Usman Putra, Lindung Wibowo. "A numerical study of the comparison of normal concrete and light weight concrete exterior beamcolumn joints behavior to cyclic lateral loads", Journal of Applied Engineering Science, 2022 Publication	<1 %
9	Qian Gu, Duanfeng Zhao, Junfeng Li, Bo Peng, Qing Deng, Shui Tian. "Seismic performance of T-shaped precast concrete superposed shear walls with cast-in-place boundary columns and special boundary elements", Journal of Building Engineering, 2021 Publication	<1 %
10	pureportal.coventry.ac.uk Internet Source	<1 %
11	patents.justia.com Internet Source	<1 %
12	Jianxing Sun, Mengyao Ci, Guangda Xu, Rucheng Wang, Weibin Ni, Zongmei Xu, Shaojie Wang. "Progressive Failure of Precast Shear Wall Structure for RC Composite Column Confined Uniform Hollow Panels under Cyclic Loading", KSCE Journal of Civil Engineering, 2023 Publication	<1 %

13	Nurjannah Aisyah, S Saloma, H Hanafiah, Putri Darin, Albimanzura Satria. "Numerical analysis of lightweight concrete wall panels having a variation of dimensions and openings that were subjected to static lateral loads", Journal of Applied Engineering Science, 2022 Publication	<1 %
14	Chao Zhang, Santosa Wongso, Hao Wang, Weiyuan Huang, Fei Shi, Xuesong Deng, Zhicheng Liang. "Seismic responses of infill walls with sliding joints and openings in semi-rigid steel frame", Journal of Building Engineering, 2022 Publication	<1 %
15	Submitted to University College London Student Paper	<1 %
16	Bin Wang, Guang Huo, Yongfeng Sun, Shansuo Zheng. "Hysteretic Behavior of Steel Reinforced Concrete Columns Based on Damage Analysis", Applied Sciences, 2019 Publication	<1 %
17	Soo-Kyoung Ha, Guk-Won Son, Sung-Yong Yu,. "Modified Stut-Tie Model Analysis of Existing Reinforced Concrete Partially Infilled Frame by U-Type Precast Wall Panel", Journal of the Korean Society for Advanced Composite Structures, 2017	<1 %

	Publication	
18	fdocuments.us Internet Source	<1 %
19	Submitted to University of Nottingham Student Paper	<1 %
20	Junchao Fan, Junhai Zhao. "Experimental investigation and analytical modeling of steel beam-to-CFDST column connection", Journal of Constructional Steel Research, 2022 Publication	<1 %
21	link.springer.com Internet Source	<1 %
22	www.1.m.growingscience.com Internet Source	<1 %
23	www.iitk.ac.in Internet Source	<1 %
24	Wilson, J.L.. "Performance of precast concrete load-bearing panel structures in regions of low to moderate seismicity", Engineering Structures, 200807 Publication	<1 %
25	core.ac.uk Internet Source	<1 %
26	Liang Bai, Chao Hou, Mingwei Cao, Jiarui Hu, Tianhua Zhou, Huilin Wei. "Cyclic performance of steel moment frames with prefabricated RC	<1 %

and ECC wall panels", Engineering Structures, 2021
Publication

27	Seyed Mohammad Hosseini, Davood Mostofinejad, Alireza Saljoughian, Bahareh Nader Tehrani. "Seismic Retrofit of Square RC Short Columns with Shear-Flexural Failure Mode via CFRP Composites Using Different Confinement Techniques", Journal of Composites for Construction, 2020 Publication	<1 %
28	lup.lub.lu.se Internet Source	<1 %
29	"High Tech Concrete: Where Technology and Engineering Meet", Springer Science and Business Media LLC, 2018 Publication	<1 %
30	Arsalan Niroomandi, Stefano Pampanin, Rajesh P. Dhakal, Mohammad Soleymani Ashtiani, Roger Nokes. "Experimental study on the effects of bi‐directional loading pattern on rectangular reinforced concrete walls", Earthquake Engineering & Structural Dynamics, 2021 Publication	<1 %
31	Basic Principles of Concrete Structures, 2016. Publication	<1 %

Exclude quotes	Off	Exclude matches	Off
Exclude bibliography	On		